

Projected increase in El Niño-driven tropical cyclone frequency in the Pacific

Savin S. Chand^{1*}, Kevin J. Tory², Hua Ye² and Kevin J. E. Walsh³

The El Niño/Southern Oscillation (ENSO) drives substantial variability in tropical cyclone (TC) activity around the world^{1–3}. However, it remains uncertain how the projected future changes in ENSO under greenhouse warming^{4–8} will affect TC activity, apart from an expectation that the overall frequency of TCs is likely to decrease for most ocean basins^{9–11}. Here we show robust changes in ENSO-driven variability in TC occurrence by the late twenty-first century. In particular, we show that TCs become more frequent (~20–40%) during future-climate El Niño events compared with present-climate El Niño events—and less frequent during future-climate La Niña events—around a group of small island nations (for example, Fiji, Vanuatu, Marshall Islands and Hawaii) in the Pacific. We examine TCs across 20 models from the Coupled Model Intercomparison Project phase 5 database¹², forced under historical and greenhouse warming conditions. The 12 most realistic models identified show a strong consensus on El Niño-driven changes in future-climate large-scale environmental conditions that modulate development of TCs over the off-equatorial western Pacific and the central North Pacific regions. These results have important implications for climate change and adaptation pathways for the vulnerable Pacific island nations.

The impact of climate change on TC activity is a topic of considerable scientific and socio-economic importance. With a few exceptions^{13,14}, most climate modelling studies have reported a likely decrease in the globally averaged TC frequency by the late twenty-first century in response to greenhouse warming^{9–11}. However, future projections of regional-scale TC activity are complicated by model deficiencies and biases¹⁵ that limit adequate simulation of regional changes in large-scale environmental conditions necessary for TC formation^{9,10}. The use of different TC detection schemes, which may require model- or region-specific tuning, further contributes to uncertainties in the regional-scale projections^{16,17}.

Over the past few years, progress in the understanding of physical mechanisms of TC genesis processes has led to the development of a model- and region-independent metric for improved TC detection in climate models¹⁶. Considerable effort has also been made to improve climate model performance in simulation of certain aspects of the climate system such as ENSO^{4–8} that strongly modulate regional changes in large-scale environmental conditions that affect TC formation. Given that future changes in the climate system as a result of anthropogenic global warming seem inevitable¹⁸, any substantial change in the character of ENSO in response to global warming—either a change in the mean state such as weakening of the Walker circulation^{19,20} or a change in the nature and frequency of ENSO variability^{4,7,8}—is likely to have a substantial impact on regional-scale TC development.

Recent studies provide consistent projections of future changes in certain aspects of ENSO using current-generation climate models^{4,6–8}. This includes an increased frequency of extreme El Niño events (such as the events of 1982/83 and 1997/98) due to more occurrences of atmospheric convection in the eastern Pacific region⁴, as well as a potential increase in the frequency of the ‘Modoki-type’ central Pacific El Niño events^{6–8}. Regardless, there is a very high expectation that ENSO variability will continue to dominate regional-scale climate in the future^{6,19}, and strongly influence weather-related variables such as rainfall in the changing climate^{6,21}. Whether such future changes in ENSO will affect regional TC activity—and if so, how—has not yet been addressed. This paper uses a suite of Coupled Model Intercomparison Project phase 5 (CMIP5) climate model simulations (Supplementary Table 1) under the historical and greenhouse warming (representative concentration pathway 8.5; RCP8.5) conditions¹² to investigate projected future changes in ENSO-driven TC frequency at the regional scale, particularly in the Pacific where the impact of ENSO is large.

We start by assessing the influence of the two main phases of ENSO²²—El Niño and La Niña (Supplementary Table 2)—on regional TC genesis locations and frequency using the 12 CMIP5 models that most realistically simulated climatological characteristics (Supplementary Figs 1 and 2) and ENSO-related variability of TCs (Supplementary Table 3; see Methods for model selection). This assessment is imperative as the ability of CMIP5 models to reproduce ENSO-driven TC variability has not yet been formally evaluated. While a few recent studies have examined the relationship using current-generation climate models, these studies were either basin-specific²³ or confined to high-resolution single-model experiments^{24,25}. The recent availability of the new generation of coupled climate models from the CMIP5 experiments has provided opportunities to examine ENSO and ENSO-driven TC variability in more detail than before.

Figure 1 shows the observed²⁶ (Fig. 1a,b) and the multimodel-mean composites (Fig. 1d,e) of TC density estimates for El Niño and La Niña events over the period 1970–2000. It is evident from the analysis that CMIP5 models can realistically simulate spatial patterns of observed TC density estimates for El Niño and La Niña conditions, and their differences (Fig. 1c,f), reasonably well in most TC basins. An exception is in the North Atlantic Basin where TC detections in CMIP5 models are much less than the observed number of TCs as also noted in several previous studies^{14,25}. This could be potentially due to inadequate representation in climate models of the North Atlantic TC precursors such as African easterly waves, as well as poor representation of large-scale environments such as vertical wind shear and relative humidity²⁷. Regardless, the simulated spatial patterns of TC density estimates over most ocean basins are quite consistent among individual models, indicating

¹Centre for Informatics and Applied Optimization, Federation University Australia, Mount Helen, Victoria 3353, Australia. ²Research and Development Branch, Bureau of Meteorology, Melbourne, Victoria 3008, Australia. ³School of Earth Sciences, University of Melbourne, Parkville, Victoria 3010, Australia. *e-mail: s.chand@federation.edu.au

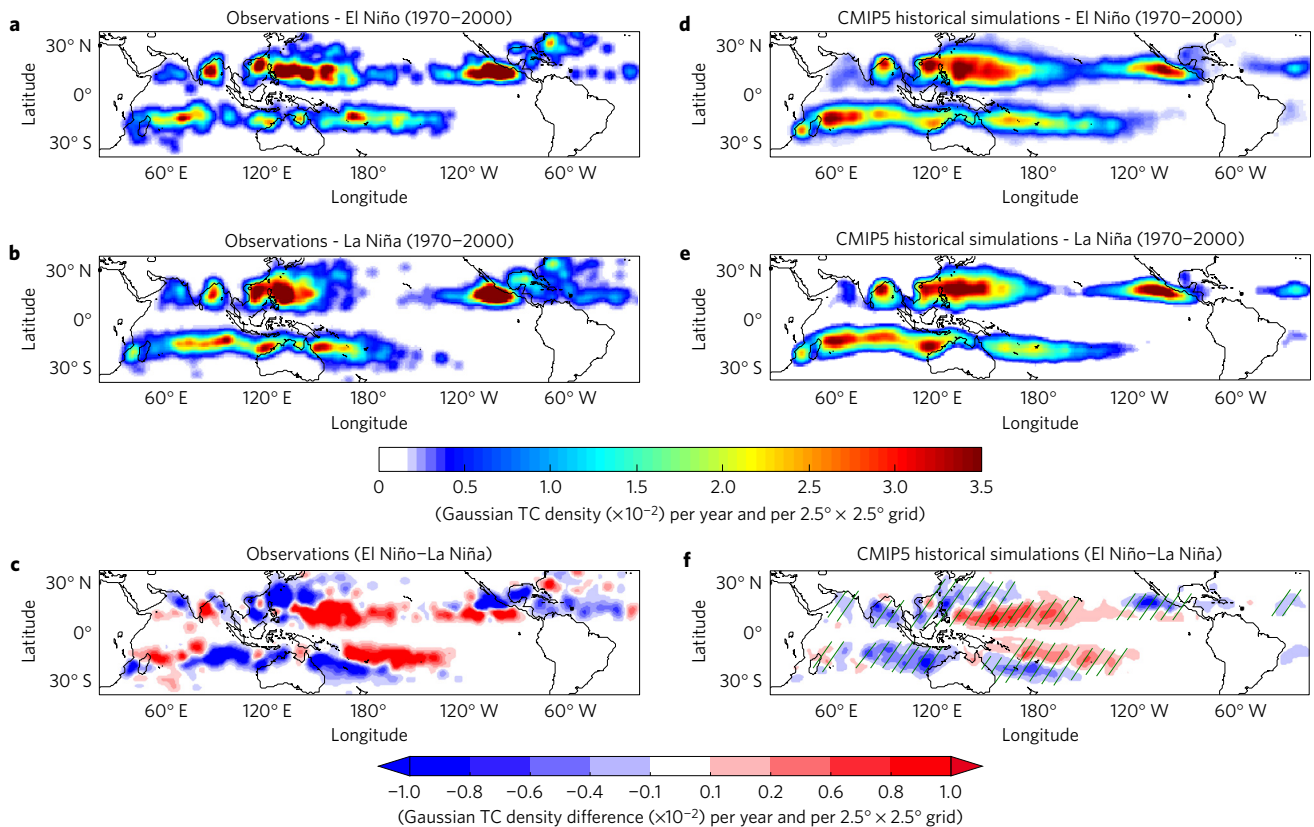


Figure 1 | Multimodel-mean composites of anisotropic Gaussian TC density estimates for El Niño and La Niña, and their differences (that is, El Niño–La Niña), at every $2.5^\circ \times 2.5^\circ$ grid box over the period 1970–2000. **a–c**, Observations. **d–f**, Historical simulations. Stippling gives an indication of the robustness (at the 95% confidence level), with at least 9 out of 12 models agreeing on the sign of change. Red shading in **c,f**, indicates enhancement of TC genesis during El Niño.

robustness of CMIP5 models (at the 95% confidence level) in simulating ENSO-driven TC variability. To further demonstrate model robustness, we verified reanalyses^{28,29} and simulated ENSO-driven changes in several large-scale environmental variables that impact TC formation, including environmental vertical wind shear, low-level cyclonic relative vorticity, sea surface temperature (SST), and mid-level relative humidity and vertical motion. Results suggest that CMIP5 models can realistically simulate ENSO-related changes in these variables that are known to be important for TC formation (Supplementary Table 3 and Supplementary Figs 3–7).

We next turn to one of the most important scientific questions on TCs and climate change. ‘How will the potential future changes in ENSO variability in a warmer world impact regional TC activity?’ It has been shown previously that the potential weakening of the Walker circulation in response to greenhouse warming²⁰ is likely to reduce mean climatological frequency of TCs by the late twenty-first century in most TC basins around the world, with a comparatively more robust decrease for the Southern Hemisphere than for the Northern Hemisphere basins^{9,10}. Our study also shows these characteristic changes using the late twentieth- and twenty-first-century simulations from the CMIP5 experiments (Fig. 2a). This includes a robust projected decrease (~ 20 – 60%) in the mean frequency of TCs for the Southern Hemisphere basins, western North Pacific, eastern North Pacific and the Bay of Bengal, and an increase in the Arabian Sea and the central North Pacific. However, to what extent these projected changes are influenced by the changing nature of ENSO in response to greenhouse warming^{4–8} is not yet clear, even for the tropical Pacific where the impact of ENSO on TC activity is substantial^{1–3}.

Here we show—by comparing and contrasting TC genesis density in El Niño and La Niña events over the late twenty-first (that

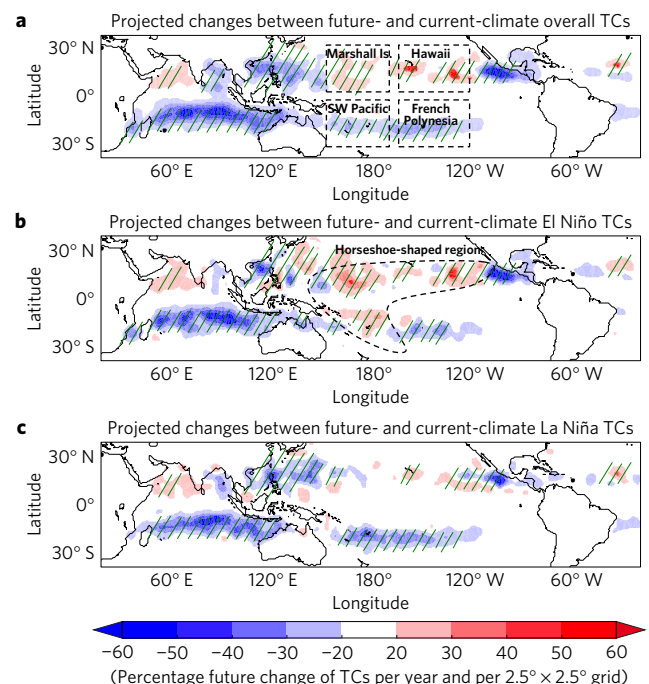


Figure 2 | Projected future changes in TC density. **a**, Overall climatology. **b**, El Niño. **c**, La Niña. Red shading indicates projected future increases in TC frequency. Stippling denotes changes that are statistically significant at the 95% level, with at least 9 out of 12 models agreeing on the sign of change. The four subregions in the Pacific, as well as the horseshoe-shaped region, that form the basis of the discussion in this paper are also indicated.

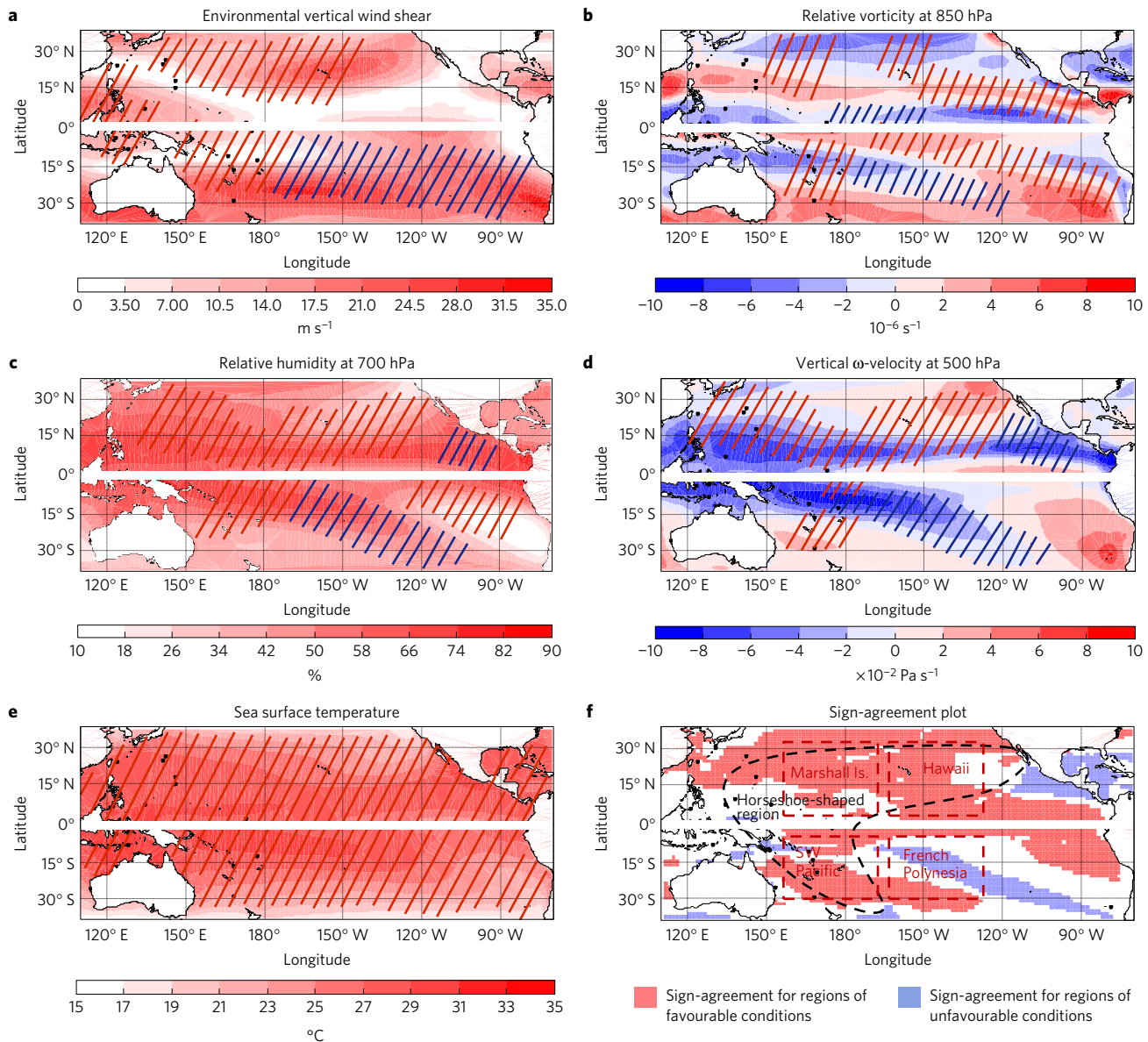


Figure 3 | December–February Southern Hemisphere and July–September Northern Hemisphere mean large-scale variables for present-climate El Niño events, and the direction of projected changes between present-climate and future-climate El Niño events. a–f, Superimposed are present-climate large-scale variables (colour shading) and regions where future changes in large-scale environmental conditions robustly favour (red stippling) and suppress (blue stippling) TC development for environmental vertical wind shear between 200 and 850 hPa (a), relative vorticity at 850 hPa (b), relative humidity at 700 hPa (c), vertical ω -velocity at 500 hPa (d), and sea surface temperature (e), and the sign-agreement plot for the regions where at least four of the five large-scale environmental variables simultaneously favour (red shading) or suppress (blue shading) increased TC development (f). Note that for clarity, the white mask at the Equator separates variables for the two different seasons used in the two hemispheres. Information used to construct this figure is obtained from Supplementary Figs 9–14 (see Supplementary Information for details).

is, 2070–2100) and twentieth century (that is, 1970–2000)—a robust projected increase (~20–40%) in TC frequency for future-climate El Niño events compared with present-climate El Niño events around the western Pacific island countries near the Date Line (for example, Fiji, Vanuatu, Samoa and Marshall Islands), and near Hawaii in the central North Pacific (Fig. 2b and Supplementary Fig. 8 shows the geographical locations of these countries). Note that regions of increased El Niño-driven TC frequency changes define a ‘horseshoe’ pattern in the Pacific (hereafter referred to as the ‘horseshoe-shaped region’, Fig. 2b). On the other hand, for future-climate La Niña events, TC frequency is projected to decrease significantly in the southwest Pacific (~20–60%) and near the Marshall Islands with no significant change near Hawaii (Fig. 2c). These results indicate the importance

of isolating ENSO-driven changes in TC frequency for regional-scale projections, particularly in the Pacific where future projections of TCs may differ significantly between the different ENSO phases.

Empirical analyses of large-scale environmental variables from the historical and RCP8.5 scenarios are performed to understand projected changes in ENSO-driven TC frequency over the Pacific (Fig. 3 and Supplementary Figs 9–14). Here, for ease of interpretation, we divide the Pacific Basin into four subregions as indicated in Fig. 2a: southwest Pacific, French Polynesia, Marshall Islands and Hawaii. Analyses reveal that for future-climate El Niño events compared with present-climate El Niño events, reduced environmental vertical wind shear (Fig. 3a) and enhanced low-level cyclonic relative vorticity (Fig. 3b) in the southwest Pacific region, particularly equatorward where most

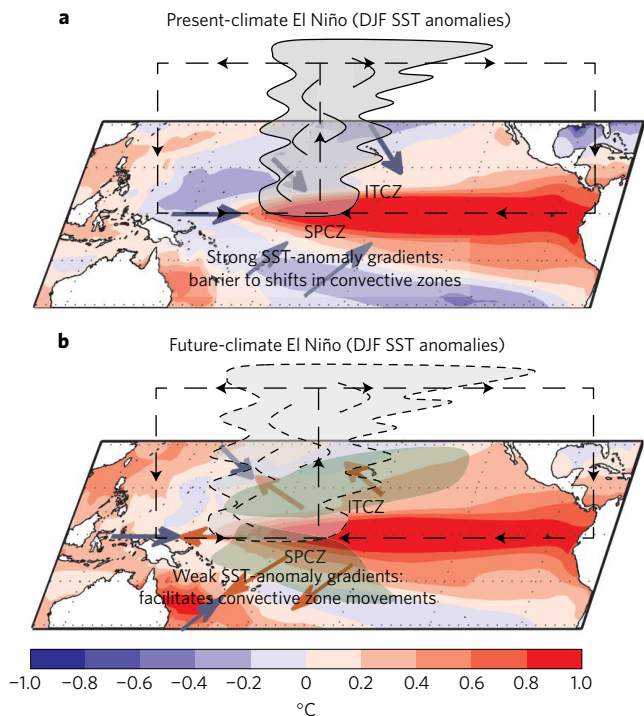


Figure 4 | Schematic illustration of a mechanism for increased TC formation in the 'horseshoe-shaped' region in the western Pacific during future-climate El Niño events compared with the present-climate El Niño events. a, b. DJF SST anomalies (colour shading) and the associated mean location of the Walker circulation for the present-climate (a) and the future-climate (b) El Niño conditions are examined. In the present-climate El Niño condition, anomalous warming of SSTs in the equatorial eastern Pacific and anomalous cooling in the western Pacific over the 'horseshoe-shaped' region creates stronger horizontal SST-anomaly gradients, confining the atmospheric convective zones in the eastern Pacific (indicated by blue arrows). However, in the future-climate El Niño events, a marked increase in anomalous warming occurs along the 'horseshoe-shaped' region in response to greenhouse warming. This reduces the overall SST-anomaly gradients, further disrupting the Walker circulation and facilitating shifts in convective zones (determined by 850-hPa convergence; green shading) into a wider area in the western Pacific (indicated by red arrows).

TC precursors form², create a more conducive environment for TC development. Increased mid-level relative humidity (Fig. 3c) and ascending motion (Fig. 3d), as well as increased SSTs (Fig. 3e), further support enhanced TC development in the southwest Pacific. However, in the French Polynesia region where typically very few TCs form anyway, unfavourable environmental vertical wind shear and relative vorticity in future-climate El Niño events appear to be the main factors further inhibiting TC development. Near the Marshall Islands and Hawaii, all large-scale variables are projected to be more favourable for TC development during future-climate El Niño events than during present-climate El Niño events (see Fig. 3f for regions where favourable environmental conditions exist simultaneously). In contrast, for future-climate La Niña events, increased environmental vertical wind shear and reduced mid-level relative humidity and ascending motion, account for a robust projection of decreased TC frequency in the southwest Pacific, French Polynesia and Marshall Islands (Supplementary Figs 9–14).

Figure 4 depicts schematically a proposed mechanism for the El Niño-driven enhancement of large-scale environmental conditions—and hence, the associated increase in TC frequency—over the 'horseshoe-shaped' region. During typical present-climate El Niño conditions, anomalous warming of SSTs in the equatorial

eastern Pacific and anomalous cooling in the western Pacific over the 'horseshoe-shaped' region creates stronger horizontal SST-anomaly gradients (Fig. 4a). Consequently, this confines the dominant atmospheric convection zone associated with the Walker circulation east of the Date Line, while the intertropical convergence zone (ITCZ) and the South Pacific convergence zone (SPCZ) shift equatorward³⁰. However, in the future-climate El Niño events, while the spatial patterns of SST anomalies remain characteristically similar to the present-climate El Niño events, a marked increase in anomalous warming occurs along the 'horseshoe-shaped' region in the western Pacific in response to greenhouse warming (Fig. 4b and Supplementary Fig. 15). This reduces the overall SST-anomaly gradients, further disrupting the Walker circulation and facilitating shifts in convective zones over a wider area in the Pacific⁴ (that is, the mean convection zone associated with the Walker circulation broadens into the western Pacific rather than being confined to east of the Date Line, while the ITCZ and SPCZ shift farther outwards as depicted in Fig. 4b). It is hypothesized that this enhanced anomalous warming over the 'horseshoe-shaped' region during future-climate El Niño events, and its resulting impact on enhanced low-level convergence (Fig. 4b), strengthen the large-scale conditions for TC formation in a warming climate^{31,32}—and hence the occurrence of more TCs—over the small island nations that lie along the 'horseshoe-shaped' region.

We note that some CMIP5 models have a common systematic bias in which the warm ENSO-driven SST anomalies extend too far to the west in the Pacific^{4,19}. The potential impact of this bias on our results is assessed by repeating the analysis: using only models that robustly simulated ENSO and the associated large-scale conditions for the Pacific; and using a statistical bias correction method outlined in ref. 6 (see also Methods for details). Overall, both methods provide stronger evidence of increased TC frequency during future-climate El Niño events over the horseshoe-shaped region (Supplementary Figs 16–19). This indicates that our major conclusions should apply to future generations of models with smaller biases.

Methods

Methods, including statements of data availability and any associated accession codes and references, are available in the [online version of this paper](#).

Received 14 October 2015; accepted 14 November 2016; published online 19 December 2016

References

- Camargo, S. J., Sobel, A. H., Barnston, A. G. & Philip, J. K. In *Global Perspectives on Tropical Cyclones: From Science to Mitigation* (eds Chan, J. C. L. & Kepert, J. D.) 325–360 (World Scientific, 2010).
- Chand, S. S. & Walsh, K. J. E. Tropical cyclone activity in the Fiji region: spatial patterns and relationship to large-scale circulation. *J. Clim.* **22**, 3877–3893 (2009).
- Ramsay, H. A., Leslie, L. M., Lamb, P. J., Richman, M. B. & Leplatrier, M. Interannual variability of tropical cyclones in the Australian region: role of large-scale environment. *J. Clim.* **21**, 1083–1103 (2008).
- Cai, W. *et al.* Increasing frequency of extreme El Niño events due to greenhouse warming. *Nat. Clim. Change* **4**, 111–116 (2014).
- Collins, M. *et al.* The impact of global warming on the tropical Pacific Ocean and El Niño. *Nat. Geosci.* **3**, 391–397 (2010).
- Power, S., Delage, F., Chung, C., Kociuba, G. & Keay, K. Robust twenty-first-century projections of El Niño and related precipitation variability. *Nature* **502**, 541–545 (2013).
- Yeh, S.-W. *et al.* El Niño in a changing climate. *Nature* **461**, 511–514 (2009).
- Kim, S. T. & Yu, J.-Y. Two types of ENSO in CMIP5 models. *J. Geophys. Res.* **39**, L11704 (2012).
- Knutson, T. R. *et al.* Tropical cyclones and climate change. *Nat. Geosci.* **3**, 157–163 (2010).
- Murakami, H., Hsu, P.-C., Arakawa, O. & Li, T. Influence of model biases on projected future changes in tropical cyclone frequency of occurrence. *J. Clim.* **27**, 2159–2181 (2014).

11. Tory, K. J., Chand, S. S., McBride, J. L., Ye, H. & Dare, R. A. Projected changes in late twenty-first-century tropical cyclone frequency in 13 coupled climate models from Phase 5 of the Coupled Model Intercomparison Project. *J. Clim.* **26**, 9946–9959 (2013).
12. Taylor, K. E., Stouffer, R. J. & Meehl, G. A. An overview of CMIP5 and the experimental design. *Bull. Am. Meteorol. Soc.* **93**, 485–498 (2012).
13. Emanuel, K. A. Downscaling CMIP5 climate models shows increased tropical cyclone activity over the 21st century. *Proc. Natl Acad. Sci. USA* **110**, 12219–12224 (2013).
14. Camargo, S. J. Global and regional aspects of tropical cyclone activity in the CMIP5 models. *J. Clim.* **26**, 9880–9902 (2013).
15. Wang, C., Zhang, L., Lee, S.-K., Wu, L. & Mechoso, C. R. A global perspective on CMIP5 climate model biases. *Nat. Clim. Change* **4**, 201–205 (2014).
16. Tory, K. J., Dare, R. A., Davidson, N. E., McBride, J. L. & Chand, S. S. The importance of low-deformation vorticity in tropical cyclone formation. *Atmos. Chem. Phys.* **13**, 2115–2132 (2013).
17. Horn, M. *et al.* Tracking scheme dependence of simulated tropical cyclone response to idealized climate simulations. *J. Clim.* **27**, 9197–9213 (2014).
18. Peters, G. P. *et al.* The challenge to keep global warming below 2 °C. *Nat. Clim. Change* **3**, 4–6 (2013).
19. Christensen, J. H. *et al.* in *Climate Change 2013: The Physical Science Basis* (eds Stocker, T. F. *et al.*) 1217–1308 (IPCC, Cambridge Univ. Press, 2013).
20. Vecchi, G. A. & Soden, B. J. Global warming and the weakening of the tropical circulation. *J. Clim.* **20**, 4316–4340 (2007).
21. Stevenson, S. *et al.* Will there be a significant change to El Niño in the twenty-first century? *J. Clim.* **25**, 2129–2145 (2012).
22. Trenberth, K. E. The definition of El Niño. *Bull. Am. Meteorol. Soc.* **78**, 2771–2777 (1997).
23. Wang, H. *et al.* How well do global climate models simulate the variability of Atlantic tropical cyclones associated with ENSO? *J. Clim.* **27**, 5673–5692 (2014).
24. Bell, R., Hodges, K., Vidale, P. L., Strachan, J. & Roberts, M. Simulation of the global ENSO–tropical cyclone teleconnection by a high-resolution coupled general circulation model. *J. Clim.* **27**, 6404–6422 (2014).
25. Kim, H.-S. *et al.* Tropical cyclone simulation and response to CO₂ doubling in the GFDL CM2.5 high-resolution coupled climate model. *J. Clim.* **27**, 8034–8054 (2014).
26. Knapp, K. R., Kruk, M. C., Levinson, D. H., Diamond, H. J. & Neumann, C. J. The International Best Track Archive for Climate Stewardship (IBTrACS) unifying tropical cyclone data. *Bull. Am. Meteorol. Soc.* **91**, 363–376 (2010).
27. Shaman, J. & Maloney, E. D. Shortcomings in climate model simulations of the ENSO–Atlantic hurricane teleconnection. *Clim. Dynam.* **38**, 1973–1988 (2012).
28. Kalnay, E. *et al.* The NCEP/NCAR 40-Year reanalysis project. *Bull. Am. Meteorol. Soc.* **77**, 437–471 (1996).
29. Rayner, N. A. *et al.* Global analyses of SST, sea ice and night marine air temperature since the late nineteenth century. *J. Geophys. Res.* **108**, 4407 (2003).
30. Widlansky, M. J. *et al.* Changes in South Pacific rainfall bands in a warming climate. *Nat. Clim. Change* **3**, 417–423 (2013).
31. Cai, W. *et al.* ENSO and greenhouse warming. *Nat. Clim. Change* **5**, 849–859 (2015).
32. Johnson, N. C. & Xie, S.-P. Changes in the sea surface temperature threshold for tropical convection. *Nat. Geosci.* **3**, 842–845 (2010).

Acknowledgements

This project is supported through funding from the Australian Government's National Environmental Science Programme (NESP). We thank S. Power, A. Dowdy, M. Wheeler and E. Ebert from the Australian Bureau of Meteorology for their valuable feedback. S.S.C. also thanks P. Vamplew and colleagues at Federation University Australia for their comments on this work.

Author contributions

S.S.C. conceived and designed the study in discussion with K.J.T. and K.J.E.W., and wrote the initial draft of the paper. S.S.C., K.J.T. and H.Y. performed the analysis. All authors contributed to interpreting results, discussion of the associated dynamics, and improvement of this paper.

Additional information

Supplementary information is available in the [online version of the paper](#). Reprints and permissions information is available online at www.nature.com/reprints. Correspondence and requests for materials should be addressed to S.S.C.

Competing financial interests

The authors declare no competing financial interests.

Methods

Data. Observed TCs are from the IBTrACS database²⁶ for the period 1970–2000. The SST data are from Hadley Centre Sea Ice and Sea Surface Temperature version 1 data set²⁹. Atmospheric variables are the National Center for Environmental Prediction–National Center for Atmospheric Research Reanalysis 1 products²⁸.

TC detection method. TCs are detected directly in climate models using the Okubo–Weiss–Zeta parameter methodology^{16,33}. This method identifies the core of quasi-closed circulations³⁴ in which TCs form. The advantage of this detection method over other traditional methods^{35–40} is that it does not need to fully resolve a TC-like circulation to identify a TC but instead detects the immediate large-scale environmental conditions in which TCs form^{41,42}. As such the method is applied to climate models without the need for threshold adjustments to match model resolutions (see also Supplementary Section 1 for details).

ENSO characterization in CMIP5 models. Despite significant advances in climate models, simulating realistic ENSO characteristics is still a challenge in models, largely associated with the difficulty in representing multiple competing feedback processes^{5,31,43–46}. Regardless, some CMIP5 models do a better job than others to accurately simulate both ENSO characteristics and the underlying atmospheric feedbacks^{43,44}, and have lower biases than in an equivalent group of CMIP3 models⁴⁶.

Classifying ENSO events in models is challenging, as models contain spatial SST biases. However, defining model-specific ENSO classifications to take into account model biases introduces subjective decisions that would make comparisons between models and with observations more difficult⁴⁵. Here we adopt a method similar to ref. 46 that utilizes the standard deviations, σ , of the Niño 3.4 index (that is, area-averaged SST anomalies over the region 5° N–5° S, 120°–170° W) to classify ENSO into El Niño and La Niña events. In this study, the $\pm 0.5\sigma$ threshold was initially chosen as it gave the best statistical match (at 95% significance level—see ref. 47) between ENSO events calculated from HadISST data and the observed records for the period 1970 to 2000. A stricter threshold of $\pm 1\sigma$ is also applied for verification purposes (see Supplementary Section 2 for details on ENSO characterization in CMIP5 models).

Note that the Niño 3.4 index used here can collectively define conventional ENSO events as well as ‘Modoki El Niños’ (sometimes referred to as central Pacific El Niños). For the purpose of this study, we do not seek to distinguish between different types of El Niño and their impacts on TCs as most CMIP5 models still have biases and deficiencies in realistically simulating the observed structure of ‘Modoki-type’ events^{6,45} as opposed to simulating conventional El Niños where CMIP5 models have improved substantially^{6,43–46}. It should be emphasized that ‘Modoki’ and conventional El Niños can have different impacts on TCs in the Pacific^{48,49}.

CMIP5 models. The CMIP5 models are chosen on the basis of their ability to realistically simulate ENSO, and ENSO-related TC climatology over the period 1970–2000. A suite of 20 CMIP5 models were initially examined using rigorous statistical approaches, such as the ‘S-statistic’ skill score^{50–52}, but only 12 satisfied the required criteria (see Supplementary Section 4 for details). These 12 models are analysed for two scenarios: historical and ‘business as usual’ RCP8.5. The historical—or the ‘twentieth-century’—simulations in CMIP5 experiments are based on realistic natural and anthropogenic forcings that cover much of the industrial period from midnineteenth century to near present. The RCP8.5 simulations are based on increasing radiative forcing throughout the twenty-first century before reaching a relative maximum value of 8.5 W m^{−2} by the end of the century¹².

Projections of future changes in ENSO-driven TC variability are evaluated using the last 30-year simulations of the twentieth (July 1970 to June 2000) and the twenty-first (July 2070 to June 2100) centuries. The 30-year historical simulation coincides with the era after which routine satellite observations of TCs became available allowing reliable comparisons of the simulated and observed TCs.

Isolating ENSO-related TC variability. After selecting objectively the ‘best-performing’ CMIP5 models, regional-scale annual TC detections from each model are binned into appropriate ENSO phases that existed during that year (that is, El Niño or La Niña—see above for ENSO characterization in CMIP5 models); years that did not fall into the two main phases were classified neutral, and TC detections from those years were not used in the analysis.

Although ENSO generally peaks in the Southern Hemisphere summer seasons (that is, December–February), its impact on TC activity can begin several months in advance from the point of onset or earlier (see ref. 1 for a review). For example, in the western North Pacific where TCs can form throughout the year, the early onset of El Niño can have a significant impact on regional-scale TC activity, particularly over the South China Sea⁵³. Similarly in the southwest Pacific Basin, TCs can form as early as October during strong El Niño events⁵⁴. To capture the

optimal degree of the ENSO–TC relationship for different TC basins, we examined the lagged statistical correlation between annual TC counts and the three-monthly mean Niño 3.4 index (Supplementary Fig. 20).

The overall ENSO–TC modulation in most TC basins begins as early as May–July and continues over the peak ENSO period of December–February (DJF). For the Southern Hemisphere basins, a TC season is spread over the two calendar years (that is, from July of the first year to June of the second year), with the peak seasonal TC activity occurring over the DJF period. This peak TC activity coincides with the peak ENSO period of DJF (see Supplementary Fig. 21 for seasonal distribution of TCs in different TC basins). Therefore, a decision was made to use the mean DJF Niño 3.4 SST anomalies for the respective models as an index of ENSO events for the Southern Hemisphere basins.

For the Northern Hemisphere basins, seasonal TC activity is spread over one calendar year (that is, from January to December) with the peak activity occurring during the July–September (JAS) period for most basins (Supplementary Fig. 21). Since this peak TC activity—generally for the Pacific basins—has a strong statistical relationship with the JAS ENSO (Supplementary Fig. 20), a decision was made to use the mean JAS Niño 3.4 SST anomalies for the respective models as an index of ENSO events for the Northern Hemisphere basins.

Multimodel ensembles in probabilistic TC projection. Multimodel composites of TC genesis locations are determined for El Niño and La Niña phases in both historical and RCP8.5 simulations. For ease of comparison, the multimodel composites are represented using TC densities to describe the spatial distribution of TC genesis in the two ENSO phases. Here TC densities are obtained by smoothing TC genesis counts in each spatial 2.5° × 2.5° grid box using probability density functions computed from an anisotropic Gaussian distribution. The constructed density estimate can then be used as a statistical representation of a larger population distribution, thus to some extent minimizing uncertainties in quantitative evaluation of projected changes for regions where TC numbers are low (see Supplementary Section 4 for details).

Some studies have considered single-model perturbed physics experiments to quantify model uncertainties (see ref. 55). This method is very useful in quantifying climate change or climate model parameters in a probabilistic sense, particularly for small-scale processes of the climate system that cannot be resolved explicitly. However, this approach—in addition to its enormous computation capacity—may also be limited in its ability to capture the full range of uncertainties in the models’ representation of the true climate system, as there are many ways to design a parameterization⁵⁶.

Here we argue that quantification of model uncertainty can be achieved through a more general approach on the basis of computing multimodel ensembles. We do recognize that CMIP5 models may not be entirely independent of each other, and that model interdependence may complicate the interpretation of multimodel ensembles. Ref. 57 derived a ‘family tree’ of CMIP5 models documenting similarities between models due to similarities in codes or the institutions producing them. Therefore, all our statistical analysis takes into account model independence (see below, as well as Supplementary Information).

Statistical significance tests. In our analysis, results are considered statistically robust if large proportions of models agree on the sign and magnitude of the change. A statistical significance test to evaluate the robustness is determined at the 5% level under the assumption that models are independent⁶. Here we have a total of 12 models but only 7 of these are considered independent on the basis of the analysis of ref. 57. Thus, the number of models required to attain 5% level of significance (based on the binomial distribution) is 6 out of 7 independent models. However, we note that similar results on the statistical significance were obtained when at least 9 (of all 12 models) agree on the sign of change. Thus, a decision was made to use the latter for all statistical significance tests in this paper.

Data availability. All data that support the findings of this study are available from the corresponding author on request.

References

- Tory, K. J., Chand, S. S., Dare, R. A. & McBride, J. L. An assessment of a model-independent tropical cyclone detection procedure in selected CMIP3 global climate models. *J. Clim.* **26**, 5508–5522 (2013).
- Dunkerton, T. J., Montgomery, M. T. & Wang, Z. Tropical cyclogenesis in a tropical wave critical layer: easterly waves. *Atmos. Chem. Phys.* **9**, 5587–5646 (2009).
- Emanuel, K. A. & Nolan, D. S. In *26th Conf. on Hurricanes and Tropical Meteorology* (Am. Meteorol. Soc., 10A.2., 2004); <http://ams.confex.com/ams/pdfpapers/75463.pdf>
- Tippett, M. K., Camargo, S. J. & Sobel, A. H. A Poisson regression index for tropical cyclone genesis and the role of large-scale vorticity in genesis. *J. Clim.* **26**, 2335–2357 (2011).
- Menkes, C. E. *et al.* Comparison of tropical cyclogenesis indices on seasonal to interannual timescales. *Clim. Dynam.* **38**, 301–321 (2012).

38. Bruyère, C. L., Holland, G. J. & Towler, E. Investigating the use of a genesis potential index for tropical cyclones in the North Atlantic basin. *J. Clim.* **25**, 8611–8626 (2012).
39. Camargo, S. J. *et al.* Testing the performance of tropical cyclone genesis indices in future climates using the HiRAM model. *J. Clim.* **27**, 9171–9196 (2014).
40. Song, Y. *et al.* Tropical cyclone genesis potential index over the western North Pacific simulated by CMIP5 models. *Adv. Atmos. Sci.* **32**, 1539–1550.
41. McBride, J. L. & Zehr, R. Observational analysis of tropical cyclone formation. Part II: Comparison of non-developing versus developing systems. *J. Atmos. Sci.* **38**, 1132–1151 (1981).
42. Davidson, N. E., Holland, G. J., McBride, J. L. & Keenan, T. D. On the formation of AMEX Tropical Cyclones Irma and Jason. *Mon. Weath. Rev.* **118**, 1981–2000 (1990).
43. Murphy, B. F., Ye, H. & Delage, F. Impacts of variations in the strength and structure of El Niño on Pacific rainfall in CMIP5 models. *Clim. Dynam.* **44**, 3171–3186 (2015).
44. Bellenger, H. *et al.* ENSO representation in climate models: from CMIP3 to CMIP5. *Clim. Dynam.* **42**, 1999–2018 (2014).
45. Taschetto, A. S. *et al.* Cold tongue and warm pool ENSO events in CMIP5: mean state and future projections. *J. Clim.* **27**, 2861–2885 (2014).
46. Grose, M. R. *et al.* Assessment of the CMIP5 global climate model simulations of the western tropical Pacific climate system and comparison to CMIP3. *Int. J. Climatol.* **34**, 3382–3399 (2014).
47. Wilks, D. S. *Statistical Methods in the Atmospheric Sciences* Ch. 5 (Academic, 2006).
48. Chand, S. *et al.* The different impact of positive-neutral and negative-neutral ENSO regimes on Australian tropical cyclones. *J. Clim.* **26**, 8008–8016 (2013).
49. Chand, S. *et al.* Impact of different ENSO regimes on southwest Pacific tropical cyclones. *J. Clim.* **26**, 600–608 (2013).
50. Flato, G. *et al.* in *Climate Change 2013: The Physical Science Basis* (eds Stocker, T. F. *et al.*) 741–866 (IPCC, Cambridge Univ. Press, 2013).
51. Taylor, K. E. Summarizing multiple aspects of model performance in a single diagram. *J. Geophys. Res.* **106**, 7183–7192 (2001).
52. Irving, D. B. Evaluating global climate models for the Pacific island region. *Clim. Res.* **49**, 167–187 (2011).
53. Chan, J. C. L. Tropical cyclone activity over the Western North Pacific associated with El Niño and La Niña events. *J. Clim.* **13**, 2960–2972 (2000).
54. Ramage, C. S. & Hori, A. M. Meteorological aspects of El Niño. *Mon. Weath. Rev.* **109**, 1827–1835 (1981).
55. Collins, M. *et al.* A comparison of perturbed physics and multi-model ensembles: Model errors, feedbacks and forcings. *Clim. Dynam.* **36**, 1737–1766 (2011).
56. Tebaldi, T. & Knutti, R. The use of multi-model ensemble in probabilistic climate projections. *Phil. Trans. R. Soc. A* **365**, 2053–2075 (2007).
57. Knutti, R., Masson, D. & Gettelman, A. Climate model genealogy: generation CMIP5 and how we got there. *Geophys. Res. Lett.* **40**, 1194–1199 (2013).